IOPscience iopscience.iop.org

Home Search Collections Journals About Contact us My IOPscience

Time-reversal transcranial ultrasound beam focusing using a k-space method

This article has been downloaded from IOPscience. Please scroll down to see the full text article.

2012 Phys. Med. Biol. 57 901

(http://iopscience.iop.org/0031-9155/57/4/901)

View the table of contents for this issue, or go to the journal homepage for more

Download details:
IP Address: 128.103.149.52
The article was downloaded on 01/02/2012 at 01:03

Please note that terms and conditions apply.

Phys. Med. Biol. **57** (2012) 901–917 doi:10.1088/0031-9155/57/4/901

Time-reversal transcranial ultrasound beam focusing using a k-space method

Yun Jing[1], **F Can Meral**[2] **and Greg T Clement**[2]

[1] Department of Mechanical and Aerospace Engineering, North Carolina State University Raleigh, NC 27695, USA
[2] Department of Radiology, Harvard Medical School, Brigham and Womens Hospital, 75 Francis St, Boston, MA 02115, USA

E-mail: yjing2@ncsu.edu

Received 5 September 2011, in final form 19 December 2011
Published 31 January 2012
Online at stacks.iop.org/PMB/57/901

Abstract

This paper proposes the use of a k-space method to obtain the correction for transcranial ultrasound beam focusing. Mirroring past approaches, a synthetic point source at the focal point is numerically excited, and propagated through the skull, using acoustic properties acquired from registered computed tomography of the skull being studied. The received data outside the skull contain the correction information and can be phase conjugated (time reversed) and then physically generated to achieve a tight focusing inside the skull, by assuming quasi-plane transmission where shear waves are not present or their contribution can be neglected. Compared with the conventional finite-difference time-domain method for wave propagation simulation, it will be shown that the k-space method is significantly more accurate even for a relatively coarse spatial resolution, leading to a dramatically reduced computation time. Both numerical simulations and experiments conducted on an *ex vivo* human skull demonstrate that precise focusing can be realized using the k-space method with a spatial resolution as low as only 2.56 grid points per wavelength, thus allowing treatment planning computation on the order of minutes.

(Some figures may appear in colour only in the online journal)

1. Introduction

Transcranial ultrasound has been actively studied in recent years due to its many promising therapeutic applications, such as the treatment of brain tumors (Fry 1977, Jolesz *et al* 2005, Pernot *et al* 2007, Cohen *et al* 2007, Jolesz 2009, Damianou *et al* 2009, Colen and Jolesz 2010), thrombolytic stroke treatment (Behrens *et al* 2001) and drug delivery (Hynynen *et al* 2006, Kinoshita *et al* 2006). However, the skull has been a barrier to precise focusing in the brain, due to its variable and highly contrasting acoustic properties, as compared with brain tissue and skin, typically leading to severe phase aberrations. When an ultrasound beam passes through the skull without correction, the focus is generally shifted and secondary peaks can

 © 2012 Institute of Physics and Engineering in Medicine

be significantly increased. These effects degrade therapeutic performance and may potentially harm the tissue outside the desired focus.

Thanks to the development of phased arrays, several approaches have been proposed to overcome the difficulty of accurately focusing ultrasound in the brain. Clement and Hynynen (2002b) introduced a layered wavevector-frequency domain model to numerically propagate ultrasound from a hemisphere-shaped transducer through the skull using input from computerized tomography (CT) scans of the head (Clement and Hynynen 2002a) to estimate the structural and acoustic properties of the skull. While this approach (Clement and Hynynen 2002b) is well established below 1 MHz and has been applied clinically (Martin *et al* 2009, McDannold *et al* 2010), its performance is not expected to be optimal at higher frequencies, due to its incapability to take the internal structure of the skull into account (Marquet *et al* 2009). Aubry *et al* (2003) modeled the wave propagation through the skull using a finite-difference time-domain (FDTD) method, again using the CT imaging, and then time reversed the signal received outside the skull in order to create a tight focus inside the brain (Thomas and Fink 1996, Marquet *et al* 2009). In this way, the variable internal structure of the skull bone is considered. This particular method requires a second ionizing modality to facilitate the phase correction, as well as excellent registration between these two modalities. Without precise registration, the beam focusing could be suboptimal (Aubry *et al* 2003). These model-based methods can also be extremely time consuming. For example, a 2009 study by Marquet *et al* (2009) reported a 2 h computation time to perform a 3D simulation through the skull. To overcome these drawbacks, point-target-based algorithms have been proposed. For example, acoustic droplet vaporization (ADV) has been suggested as a potential *in situ* point-target for aberration correction; nevertheless, a prior injection is required (Haworth *et al* 2008) and viability *in vivo* has yet to be established. In a more recent paper (Gateau *et al* 2010), a two-step adaptive focusing technique was also investigated. In the first step, the FDTD- and CT-based phase correction method was used to introduce a cavitation bubble by a high-intensity pulse. The second step is to use the acoustic emission of the bubble to maximize the pressure amplitude at the target point.

The present study concentrates on improving the computational efficiency of the CT-based correction method. Instead of using the conventional FDTD approach, a k-space method (Mast *et al* 2001, Mast 2002, Tabei *et al* 2002, Cox *et al* 2007) is used to simulate the wave propagation through the skull. An inherent advantage of the k-space method is that it can accurately calculate the phase aberration from the skull even if a coarse mesh is used. On the other hand, FDTD needs very fine mesh to capture the phase information, which inevitably leads to a long computation time and becomes demanding of the computational resource. An efficient computational algorithm is especially useful if the ultrasound beam needs to be focused at multiple locations relatively far away from each other, and the simulation may need to be carried out multiple times.

The paper is structured as follows: in section 2, the theory of the k-space method is briefly revisited. Section 3 discusses simulation results for wave propagation through the skull using the k-space method and its application for time-reversal transcranial focusing. Section 4 presents the experimental results and section 5 concludes the paper.

2. Theory

For a fluid medium with inhomogeneous acoustic properties, the linearized acoustic wave equation can be written as

$$\rho\nabla\cdot\left(\frac{1}{\rho}\nabla p\right)-\frac{1}{c^2}\frac{\partial^2 p}{\partial t^2}+\frac{\delta}{c^4}\frac{\partial^3 p}{\partial t^3}=0, \tag{1}$$

where p is the sound pressure, c is the sound speed, δ is the sound diffusivity and ρ is the ambient density. All materials are assumed to be spatially varying functions. The equation inherently assumes a thermoviscous fluid, as the relaxation mechanism is not considered. However, it can be readily modified to include power law absorption and dispersion (Treeby and Cox 2010).

By using the normalized wave field $f = \frac{p}{\sqrt{\rho}}$ (Mast *et al* 2001), the first-order derivative term is eliminated and equation (1) becomes

$$\nabla^2 f - \frac{1}{c_0^2}\frac{\partial^2 f}{\partial t^2} = \sqrt{\rho}\nabla^2\frac{1}{\sqrt{\rho}}f + \frac{1}{c_0^2}\left(\frac{c_0^2}{c^2} - 1\right)\frac{\partial^2 f}{\partial t^2} - \frac{\delta}{c^4}\frac{\partial^3 f}{\partial t^3}, \tag{2}$$

where c_0 is the background speed of sound.

Following the approach originally described by Mast *et al* (2001), an auxiliary field is defined by $w = f + v$, where $v = \left(\frac{c_0^2}{c^2} - 1\right)f$. Equation (2) can then be reduced to

$$-\frac{1}{c_0^2}\frac{\partial^2 w}{\partial t^2} = \nabla^2 v - \nabla^2 w + (q - d)/c_0^2, \tag{3}$$

where

$$\begin{aligned} q &= c_0^2\sqrt{\rho}\nabla^2\frac{1}{\sqrt{\rho}}f, \\ d &= c_0^2\frac{\delta}{c^4}\frac{\partial^3 f}{\partial t^3}. \end{aligned} \tag{4}$$

Fourier transformations of equation (3) in the spatial domain yield the k-space equation

$$\frac{\partial^2 W}{\partial t^2} = c_0^2 k^2 (V - W) - (Q - D), \tag{5}$$

where $k = \sqrt{k_x^2 + k_y^2 + k_z^2}$, and W, V, Q and D are the spatial Fourier transforms of w, v, q and d, respectively, which can be readily calculated using a fast Fourier transform algorithm. This step is crucial, as in this way the differentiation in the wave equation is calculated by the Fourier transform as opposed to the conventional finite-difference approximation, which is known to have a relatively large linear phase error (dispersion error) (Liu 1998). On the other hand, the k-space method can be viewed as a limiting case of an infinite-order accurate finite-difference method, which theoretically only requires two nodes per wavelength to achieve exact solutions for wave equations with smoothly varying coefficients (Liu 1998).

Equation (5) can be solved in a nonstandard finite-difference approach (Mast *et al* 2001, Tabei *et al* 2002),

$$W(t + \triangle t) - 2W(t) + W(t - \triangle t) = 4\sin^2\left(\frac{c_0 k \triangle t}{2}\right)\left[V - W - \frac{1}{c_0^2 k^2}(Q - D)\right], \tag{6}$$

where $\triangle t$ is the temporal step size. The stability condition was given as (Mast *et al* 2001)

$$\sin\left(\frac{\mathrm{CFL}\, c_0 \pi}{2 c_{\max}}\right) \leqslant \frac{c_0}{c_{\max}}, \tag{7}$$

where CFL is the Courant–Friedrichs–Lewy number $c_{\max}\triangle t/\triangle x$.

To calculate D (or d), the following first-order backward difference approximation was employed:

$$\frac{\partial^3 f}{\partial t^3} = \frac{f(t) - 3f(t - \triangle t) + 3f(t - 2\triangle t) - f(t - 3\triangle t)}{\triangle t^3}. \tag{8}$$

Finally, an absorption layer is built into the algorithm to effectively eliminate the wrap-around artifact (Kosloff and Kosloff 1986, Mast 2002). The equation for the absorbing layer can be written in f as

$$\nabla^2 f - \frac{1}{c_0^2}\frac{\partial^2 f}{\partial t^2} = 2\gamma\frac{\partial f}{\partial t} + \gamma^2 f, \tag{9}$$

where γ is an absorption term (frequency independent). In this study, we have used (Kosloff and Kosloff 1986)

$$\gamma = U_0/\cosh^2(\alpha n), \tag{10}$$

where U_0 is a constant (2.0 in the present study), α is a decay factor (0.1 in the present study) and n denotes the distance in the number of grid points from the boundary. This equation was also implemented by the k-space method.

To conclude this section, it is noted that a slightly different k-space algorithm (Tabei *et al* 2002, Tillet *et al* 2009) was also proposed based on the first-order wave equations, which was shown to be more accurate when the contrast is large, but requires extra computation and storage of the particle displacement vector.

3. Numerical simulations

3.1. Evaluation of the k-space method for transcranial wave propagation

It is well known that the k-space method is highly accurate for homogeneous media or weakly inhomogeneous media even when there are only two grid points per wavelength (Mast *et al* 2001), as opposed to eight to ten grid points per wavelength required by the conventional fourth-order FDTD algorithm. However, its accuracy quickly deteriorates as the contrast in the acoustic media becomes large, which is the case for transcranial wave propagation, as the speed of sound and density are much larger than the brain tissue. Therefore, it is crucial to first test the k-space method for transcranial wave propagation with varied grid point sizes and to find the optimal spatial resolution.

In order to test the k-space wave propagation code with extremely fine spatial resolution, a 2D problem was studied. Densities in the skull were acquired from CT scans, while other acoustic properties were obtained utilizing the empirical equations (Aubry *et al* 2003, Marquet *et al* 2009),

$$\begin{aligned} \psi &= 1 - \frac{H}{1000}, \\ c &= c_{\text{water}}\psi + c_{\text{bone}}(1-\psi), \\ abs &= abs_{\min} + (abs_{\max} - abs_{\min}) \times \psi^{\beta}, \end{aligned} \tag{11}$$

where H is the Hounsfield unit, ψ is the porosity, c_{water} is the speed of sound in water, c_{bone} is the maximum speed of sound in the skull (set to be 2900 m s^{-1} here), *abs* is the absorption coefficient, and $abs_{\min}$ and $abs_{\max}$ are 0.02 and 1 dB mm^{-1}, respectively. To convert *abs* to the diffusivity δ, $\delta = abs \times 2 \times c^3/\omega^2$ was used (Hamilton and Blackstock 1998). Finally, β is set to be 0.5 (Aubry *et al* 2003). The choices for these acoustic parameters come from the available literature. For example, the cortical bone was found to have an average speed of sound around 2471 ± 90 m s^{-1} near 1 MHz (Pichardo *et al* 2011), so c_{bone} was chosen such that the average speed of sound is in this range. The minimal and maximal values for absorption used were 0.2 and 8 db mm^{-1} at 1.5 MHz (Aubry *et al* 2003). The minimal and maximal values in this study were therefore chosen to be smaller because the primary frequency in this study is lower, i.e. 1 MHz. Even though the numbers 0.02 and 1 db mm^{-1} are empirical, additional

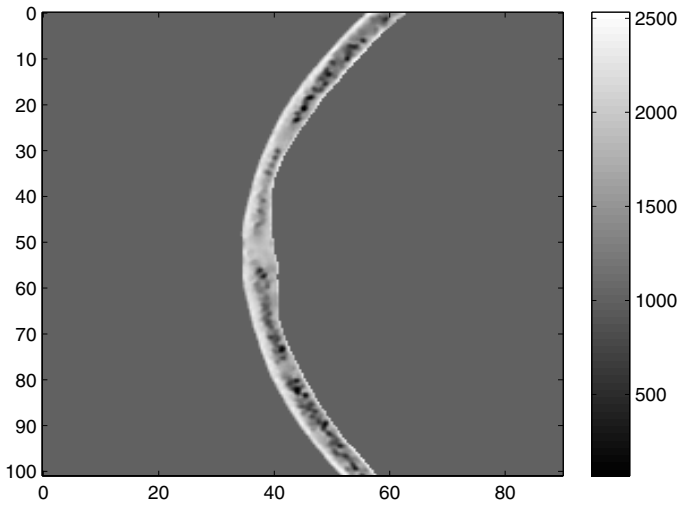

Figure 1. Density (kg m^{-3}) of one slice of the skull used for 2D simulation. The axes are in mm.

simulations considering a range of absorption coefficients yielded no significant impact on the focusing profile (side lobes, accuracy of the focusing), which is the main concern in this paper. However, it is further noted that in this section, diffusivity is not considered (set to zero). This is a necessary step since time-reversal theory is invalid if an odd-order time derivative (diffusivity in this case) exists. As will be shown later, the diffusivity is considered when simulating wave propagation from the transducer to the skull in the next section.

The current code does not simulate the shear wave propagation. Nevertheless, shear waves can be neglected when the incident angle is small ($<20^{\circ}$) (Clement *et al* 2004), which is the case in our study.

Figure 1 shows a 2D cross-section of skull density as determined from CT Hounsfield units. Note that at a few locations, the densities in the skull are smaller than the water, and there are two potential reasons: the skulls are stored in a formaldehyde solution ($\rho = 0.8$ g cm^{-3}), which may be present within bone cavities. Also, there are a few locations (e.g. the sinus cavities) that may contain air bubbles.

An 8-cycle quasi-plane wave with a center frequency of 1 MHz was first generated inside the skull, and propagated toward the outside of the skull. To mimic the experimental condition, the skull was considered to be submerged in water. Figure 2 illustrates the simulation at two different times, showing severe distortion and scattering due to the skull.

To assess the accuracy of the model as a function of spatial resolution, pressures were recorded at a fixed location outside the skull (20 mm, 38.3 mm in the coordinates of figure 1). Five different spatial resolutions were considered. The original spatial resolution given by the CT scan was 3.84 grid points per wavelength at 1 MHz in water. The wavelength λ in this case corresponds to 1.5 mm. Throughout the paper, the resolution is always calculated based on this wavelength, unless otherwise mentioned. Noting that the wavelength in the skull is generally higher than in water or tissue, this choice of a reference wavelength assures that a spatial resolution, once deemed appropriate for simulating wave propagation in water, will also be suitable for the simulation in the skull. The original slice resolution, not used in the 2D case though, was 1 mm. The acoustic properties of the skull were linearly interpolated to have 2.56, 7.68, 15.36 and 30.72 grid points per wavelength. Note that, to satisfy the Nyquist

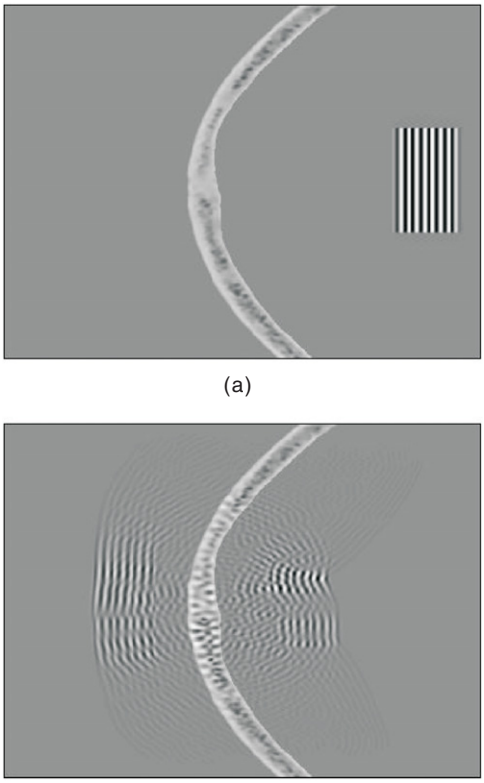

Figure 2. Propagation of a quasi-plane wave through a skull in 2D. (a) Time 0 μs, (b) time 37 μs.

frequency, the spatial resolution cannot go below two grid points per wavelength. The time step was fixed and the Courant–Friedrichs–Lewy (CFL) number, i.e. $c_{\max}\triangle t/\triangle x$, was 0.25. For comparison, an FDTD calculation was also carried out, where the spatial derivative was calculated based on a fourth-order approximation. The leap-frog algorithm was used for time stepping and the CFL number was 0.2.

Figure 3 shows the pressure calculated by the k-space method at the point of measurement. Considering the results at the highest resolution as the reference, a coarse mesh introduced some slight phase and amplitude errors. For example, for the lowest spatial resolution, the phase error is around $T/5$ where T is the period. It was predicted that these errors would be small, as compared to error caused by noise and alignment under physical conditions. This prediction will later be verified in section 4. The results seem to converge well as the spatial resolution approaches the maximum. It also appears that a spatial resolution at 7.68 grid points per wavelength may be sufficient for obtaining relatively reliable results (phase error smaller than $T/8$ (Aubry *et al* 2003)), providing a good tradeoff between computation accuracy and efficiency.

Figure 4 presents results calculated by the FDTD method. In the case of a coarse mesh, FDTD generated a result that is greatly contaminated by the phase error, which seems to dominate over any other errors. Figure 5 shows the results for both the k-space and the FDTD method for the spatial resolutions of 2.56 and 30.72 grid points per wavelength. At the spatial resolution of 30.76 grid points per wavelength, the k-space and FDTD method yield similar results. There is also excellent agreement when using 16 grid points per wavelength.

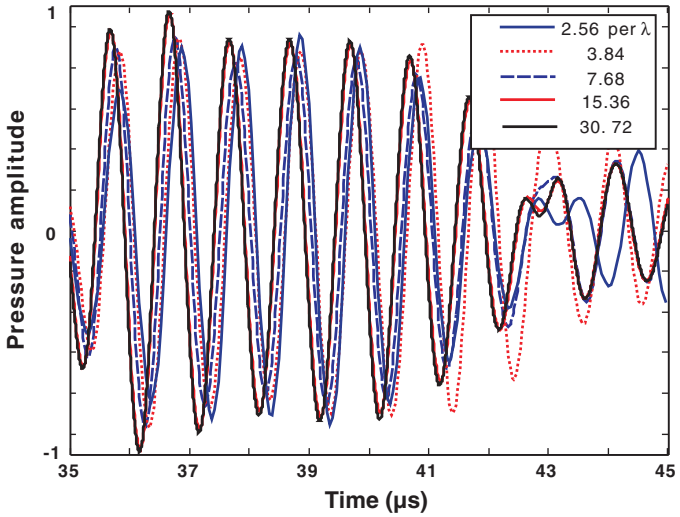

Figure 3. Acoustic pressure measured at a location outside the skull. Calculated from the k-space method with different spatial resolutions.

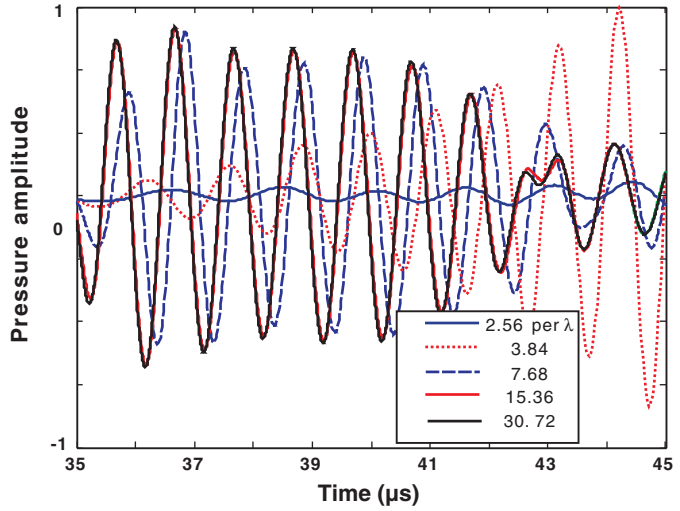

Figure 4. Acoustic pressure measured at a location outside the skull. Calculated from the FDTD method with different spatial resolutions.

In contrast, at a low spatial resolution, the FDTD method is significantly less accurate. The reason why the FDTD method at a low spatial resolution gives such low pressure amplitudes is the large dispersion error, so the large pressure amplitude can only be seen at a much later time which is not included in the current time frame.

Additional comparisons (not shown here) also indicate that the k-space method with a spatial resolution of 7.68 grid points per wavelength contains less error than the FDTD method at the same resolution, e.g., $T/8$ versus $T/6$ for phase error.

As the resolution decreases, not only does the numerical model become less accurate, but also the fine structure of the skull becomes lost. To conclude this section, we test whether or not it is necessary to model the fine structure of the skull. A 4-cycle quasi-plane wave with a

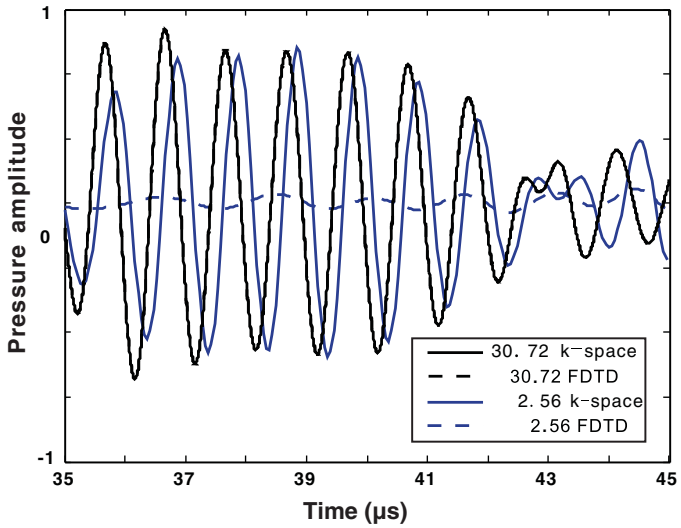

Figure 5. Comparison between the k-space and the FDTD methods for ultrasound simulation through the skull using two different spatial resolutions. One with 30.72 grid points per wavelength, and one with 2.56 grid points per wavelength.

center frequency of 400 kHz was generated inside the skull, and numerically propagated using the k-space method toward the outside of the skull. At this frequency, the original CT scan resolution is 1/9.6 of the wavelength, and the simulation is expected to be accurate without interpolations according to the study above. Two separate simulations were carried out. The first one employed the original CT scan resolution, while the second one interpolated the skull profile so that the internal structure resolution became 1/2.4 of the wavelength and then the spatial resolution was interpolated back again to be the same in the first simulation. In this case, these two simulations have the same accuracy in terms of their numerical algorithm, but the second one discarded the fine structure of the skull. Figure 6 shows the density of the skull for the second simulation, which can be directly compared with figure 1.

The sound pressure was again recorded at (20 mm, 38.3 mm) and is plotted in figure 7. It can be seen that some amplitude errors occur. However, even without considering the fine structure in the skull, the phase of the pressure can still be predicted. This is important for phase correction in transcranial focusing.

Even though only one frequency was tested here, the conclusion at 400 kHz can be extended to other frequencies. In this study, a low resolution that is 1/2.4 wavelength was employed; however, this is the wavelength in the water. The wavelength in the skull is actually larger because the speed of sound is larger, and the CT resolution is in fact approximately 1/4 wavelength in the skull, in an average sense. A microstructure that is smaller than this CT resolution, i.e. 1/4 wavelength, should not strongly affect the acoustic transmission or reflection, because it is moderately sub-wavelength. Therefore, it is expected that neglecting the fine microstructure (with a size smaller than about half of the wavelength in water) in the skull at other frequencies is also a reasonable simplification.

3.2. Phase correction using the time-reversal technique and the k-space method

To estimate the appropriate phase correction for transcranial beam focusing, a point source was excited at the desired focus, and the propagation through the skull was simulated using the

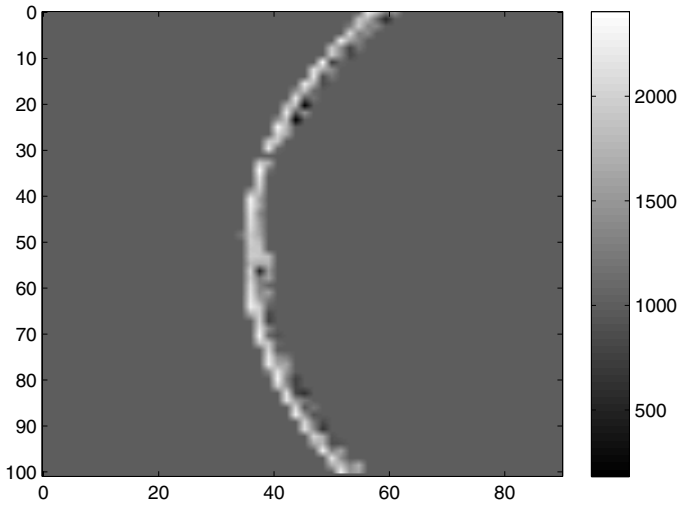

Figure 6. Density (kg m^{-3}) of one slice of the skull used for 2D simulation without the fine structure of the skull. The axes are in mm.

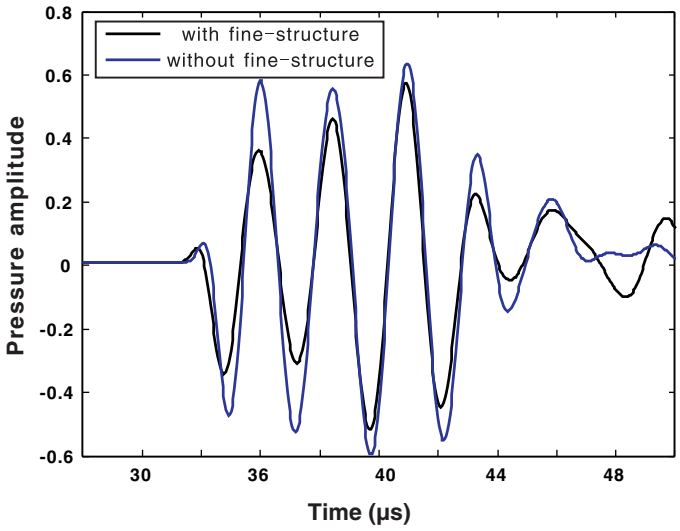

Figure 7. Acoustic pressure measured at a location outside the skull. Calculated from the k-space method with and without the internal fine structure of the skull.

FDTD method with the CT imaging as the input (Aubry *et al* 2003). The time-reversal technique utilizes the fact that the lossless wave equation only has a second-order time derivative, indicating that if $p(t)$ is a solution to the equation, $p(-t)$ is also a solution (Fink and Prada 2001). Therefore, if the received acoustic signal can be emitted in a time-reversed manner, the point source (a focal point) can be reconstructed. It has been found in the last section that the k-space method produces much less numerical error compared with the FDTD method at a low spatial resolution. Therefore, it is hypothesized that it is feasible to obtain the phase correction using the k-space method with a coarse spatial resolution. This section aims to verify this hypothesis. It is noted that the amplitude change due to the attenuation in the skull is not corrected in the current algorithm.

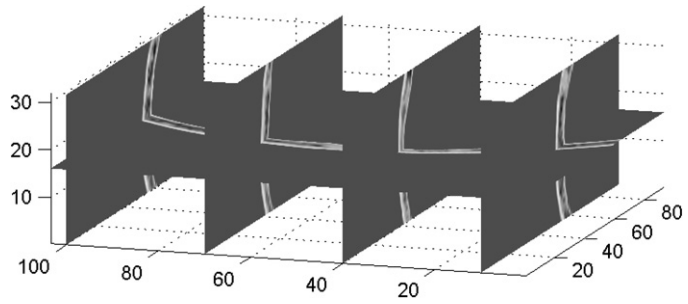

Figure 8. A 3D spatial representation of the sound speed distribution deduced from CT scans and used as input data for the full 3D simulation. The axes are in mm.

To account for the out-of-plane refraction, 3D full simulations were carried out. Figure 8 shows the portion of the 3D skull used for the simulation. The center of this portion of the skull is shown in figure 1. The focus was set at 50 mm below the skull and the virtual receivers were 10 mm away from the skull surface.

Five separate simulations using the k-space method were carried out. The first one used a fine spatial resolution (7.68 grid points per wavelength) for both backward (from inside the skull to outside) and forward (from outside the skull to inside) wave propagations. A higher spatial resolution leads to a prohibitive computational burden. Once again, the diffusivity was only considered in the forward propagation.

For the backward propagation, the computational dimension was 47 mm $\times$ 100 mm $\times$ 31 mm, and the matrix size was $241 \times 517 \times 159$. This relatively small matrix size was allowed because of the following. (1) The virtual receiver array was considered to be small, and the size approximately corresponds to the 1D array that our lab currently possesses (details can be found in section 4). (2) The propagation in the tissue can be modeled by faster simulation approaches, e.g., a ray-tracing code (Marquet *et al* 2009). Therefore, the k-space method was only applied to simulate the wave propagation through the skull and to a plane (transducer plane) close to the skull.

The second and third simulations used two relatively coarse spatial resolutions (2.56 and 3.84 grid points per wavelength) for the backward propagation and the fine spatial resolution for the forward propagation. The matrix sizes were $83 \times 171 \times 53$ and $121 \times 259 \times 77$, respectively.

The fourth simulation used the fine spatial resolution for both propagations; however, the medium was considered homogeneous in the backward propagation, i.e. the skull was not considered and no correction was applied. In the last simulation, a coarse spatial resolution (2.56 grid points per wavelength) was used for the backward propagation and the fine spatial resolution was used for the forward propagation. In this simulation, the backward propagation was implemented by FDTD.

In the second, third and last simulations, the signal outside the skull obtained from the coarse mesh-based simulation was linearly interpolated as the input to the forward propagation with the fine resolution. The fourth simulation provides a reference as to how much focus can be distorted by the phase aberration from the skull.

Figure 9 shows the pressure square distribution on the focal plane for every case considered. It can be observed that a tight focus can be generated only if phase correction is applied. The backward propagation calculated using medium (3.84 grid points per wavelength) and low (2.56 grid points per wavelength) spatial resolutions seems to be able to provide sufficient information for phase corrections, as visually there is no difference between these

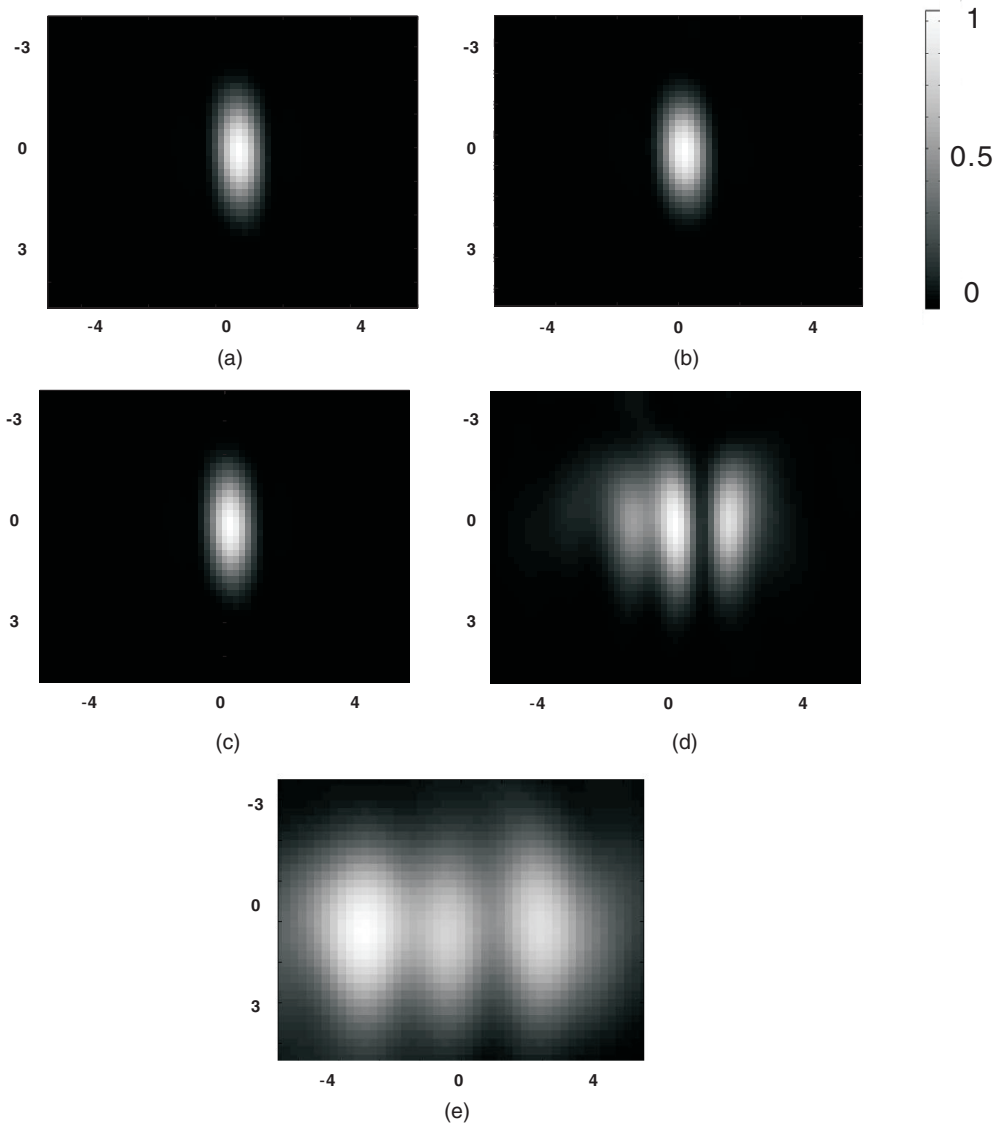

Figure 9. Normalized pressure square distribution on the focal plane. (a) With high spatial resolution for both forward and backward propagations. (b) With medium spatial resolution for backward propagation and high spatial resolution for forward propagation. (c) With low spatial resolution for backward propagation and high spatial resolution for forward propagation. (d) With high spatial resolution for both forward and backward propagations; however, the skull was not considered for the backward propagation. (e) With low-spatial resolution for backward propagation using FDTD and high spatial resolution for forward propagation. The axes are in mm.

calculations using different resolutions. On the other hand, the simulation with the low spatial resolution from FDTD shows poor focusing through the skull. To further compare these cases, figure 10 shows the pressure square distribution along a line crossing the focal point (the result with FDTD is not shown because its inaccuracy is proven in figure 9). It can be seen that the calculation with coarse spatial resolutions produces only slightly higher side lobes, while the one without considering the skull suffers from a strong defocusing effect. Overall, calculations

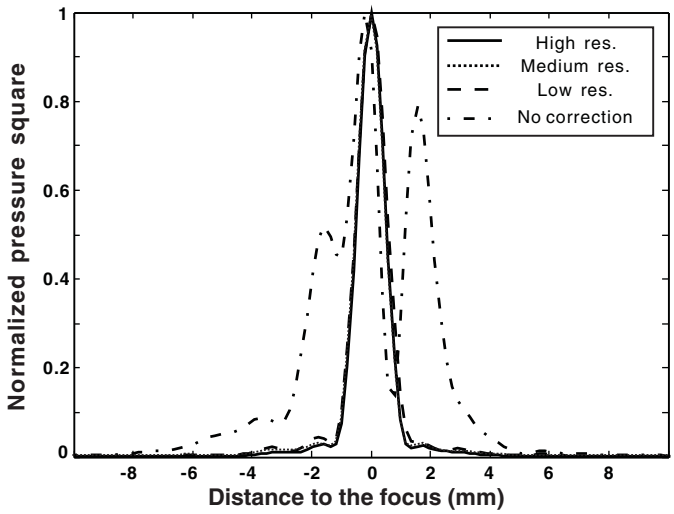

Figure 10. Pressure square distribution along a line crossing the focal point from four different calculations.

based on all resolutions can focus the ultrasound beam through the skull. However, the one with the low spatial resolution is much less time consuming, which only took 17 s. The one with the medium spatial resolution took 1.8 min and the high spatial resolution took 24 min. The algorithm was implemented using Matlab on an XP 64 bit operating system. The hardware consisted of four dual-core 2.67 GHz Xeon processors, and 24 GB of RAM.

This result is significant, as the computation time at the high spatial resolution was reduced by a factor of 84 when the low spatial resolution was used. Even for the real application where a much larger hemispherical array will be used, indicating a larger computational domain, the proposed approach can still be efficient and can potentially lead to quasi-real-time transcranial beam focusing. For the FDTD method, the computation time is similar to the k-space method for the same spatial resolution. However, as shown in figure 9, the FDTD method implemented at a low resolution produces very large errors that prevent its application for time-reversal transcranial beam focusing.

4. Experimental verifications

The goal of this section is to experimentally verify the transcranial focusing using the k-space method with a coarse spatial resolution.

4.1. Methods

Previous studies, which propose FDTD as a numerical solution method, used a 1D array for the experimental verification of the transcranial ultrasound propagation problem (Aubry *et al* 2003). In order to be consistent with these studies and for comparison, a 1D, linear ultrasound imaging transducer array (Material Systems Inc., Littleton, MA) was used in the experiments. This custom transducer is operating at frequencies ($\leqslant$ 1 MHz) lower than commercially available ultrasound probes (Meral and Clement 2010). The transducer consists of 128 linear elements, whose element width is 0.65 mm, pitch is 0.75 mm and element height in the elevation direction is 20 mm. An ultrasound engine (Verasonics, Redmond, WA) with custom

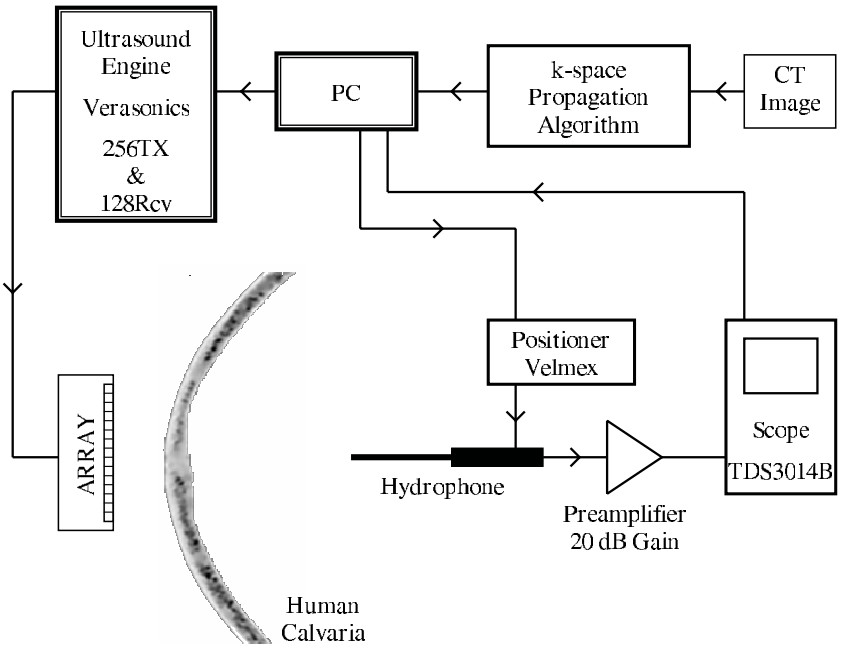

Figure 11. Schematic of the experimental setup.

modifications allowing it to perform at megahertz frequencies and below, was used to operate the transducer array. The ultrasound engine has the capability of transmitting and receiving from 128 independently controlled channels. A hydrophone (400 μm Onda Corporation, Sunnyvale, CA), mounted on a three-axis positioner system (Velmex, Bloomfield, NY), was used to scan the acoustic pressure field of a focused beam created inside the skull. The hydrophone signal was amplified by 20 dB (AH-2010, Onda Corporation, Sunnyvale, CA), recorded by a digital oscilloscope (TDS3014B, Tektronix, Inc., Beaverton, OR) and transferred to Matlab for further processing. An *ex vivo*, formalin fixed human calvaria, stored in 10% buffered formalin solution and room temperature was used in the experiments. This skull is identical to the one used in section 3 whose properties were computed from CT images. Distinct patterns of the skull geometry that were identified from the CT images were used to roughly align the skull with respect to the array as close as it was positioned in the simulations. However, the success of the numerical algorithm relies on precisely positioning the skull by constraining its three translational and three rotational degrees of freedom. The distance between the skull and transducer array (z-axis) is defined as 10 mm during the simulations; this value was maintained constant with a gauge block during positioning. The exact location of the skull section that was used in the simulations is known from CT images; based on this information the skull was positioned in the y-axis to align this section coincident with the imaging plane. Rotation of the skull about x- and y-axes was also measured from a set of CT images; these two rotation angles were also applied to the skull's position. The lateral (x-axis) position of the skull was ensured by capturing an ultrasound image of the skull with the array and comparing it with the simulation section (figure 1). Finally, the rotation of the skull around the z-axis was manually controlled, while other constraints were maintained. The hydrophone was used to scan a line of the focal plane and the skull's rotational position was iterated based on the measured pressure profile. Measurements were performed in a water tank filled with deionized water. A schematic of the experimental setup is presented in figure 11.

A simulated focused field was created inside the skull and numerically back propagated to the array which was located 10 mm away from the skull, as described in section 3. The back-propagated pressure signal was recorded at 128 different locations corresponding to the center of array elements. These signals were then time reversed to obtain the signals that needed to be transmitted from the array to create the focus inside the skull. The Verasonics system can transmit tri-state pulses at a given voltage level (+V, 0, −V); these pulses are defined by their period, duty cycle and the number of cycles. The resulting transmitted waveform is broadband and has higher order harmonics. The pulse train can be individually defined for each transmit channel. Even though it is not possible to create the simulated signals of the k-space propagation algorithm exactly, it is made sure that the phase of the transmitted signal matches the phase of the simulated signal at the center frequency, 1 MHz. The phase of the transmitted signal is computed from the simulations and converted into a time delay for each channel. Also the amplitude of an emitting channel cannot be changed during transmission, prohibiting any kind of amplitude modulation. Therefore, each channel's signal was set to a constant voltage, based on the maximum voltage it will emit. Once phase and amplitude for each channel were computed and applied, a pulse with 8 cycles at 1 MHz was emitted.

4.2. Results

The array was driven with the numerically computed focusing pulse of 8 cycles at 1 MHz center frequency and the resulting acoustic field of a focused beam inside the skull was measured for the *xz* (axial) and *xy* (focal) planes. These two orthogonal planes have the area of 16 mm × 32 mm for both *xz* and *xz* with a 0.4 mm ($< \lambda/4$) scan step size in all directions. Measured pressure data are squared and averaged in time to obtain a single pressure square value for each measurement point. Field measurements of the focused pulse based on the signals computed with a high spatial resolution k-space model, medium spatial resolution k-space model and low spatial resolution model are given in figure 12, as well as the field from signals computed without considering the skull. The first row of results presented in figure 12 belongs to the *xz*-plane and k-space propagation models with three different levels of resolution successfully restore the focus at its desired location. In the plane of consideration, the focus, instead of being a point, is an elongated strip in the axial direction due to the array geometry and specifications. The second row of results corresponds to the *xy*-plane pressure distribution results and recovered focus with three k-space propagation models can be seen. The relatively large height of the array elements (20 mm) results in a pressure distribution resembling a strip rather than a point at the focal plane.

The precision of the correction algorithm was assessed by the shape of the focus as well as the side-lobe amplitudes (Aubry *et al* 2003). Therefore, results for pressure square distribution measurements along a line crossing the focal point are given in figure 13 for examining the shape of the different foci. Again, measurement results obtained using the signals computed with four different k-space propagation models are presented. For the high spatial resolution k-space algorithm, a focal spot with a full-width at half-maximum (FWHM) of 1.84 mm, in the lateral direction, is obtained. The highest side lobe has an amplitude of −8.12 dB with respect to the main peak. For the medium spatial resolution k-space algorithm, FWHM and side-lobe amplitudes are measured as 1.86 mm and −10.03 dB, respectively. Similarly, for the focal spot based on the low spatial resolution k-space propagation model, the FWHM is 1.84 mm and the side-lobe level is −6.76 dB. The position of the focal spot shifts less than 0.4 mm, between high and low spatial resolution simulations. In the case where propagation through the skull is ignored in the k-space simulation, a split focus is observed 2.4 mm apart from each other, the second one having an amplitude of 92% of the first one. This situation could be disastrous

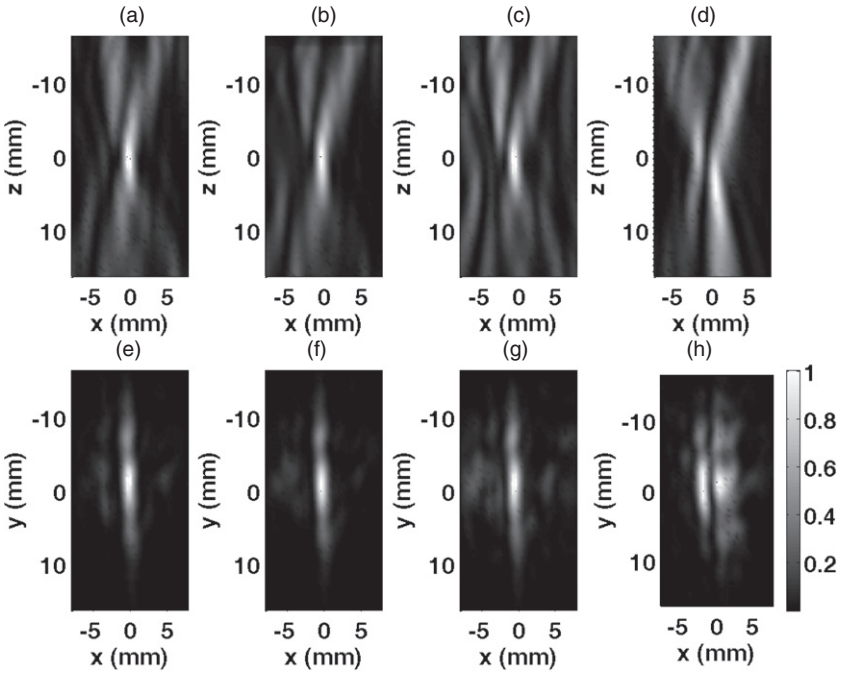

Figure 12. Normalized measurement results for the focused beam using various corrections methods. (a) Scan of the axial plane (x–z) using the high-resolution k-space method, (b) medium-resolution k-space method, (c) low-resolution k-space method and (d) without considering the skull. Focal plane (x–y) measurements using (e) high-resolution k-space method, (f) medium-resolution k-space method, (g) low-resolution k-space method and (h) without considering the skull.

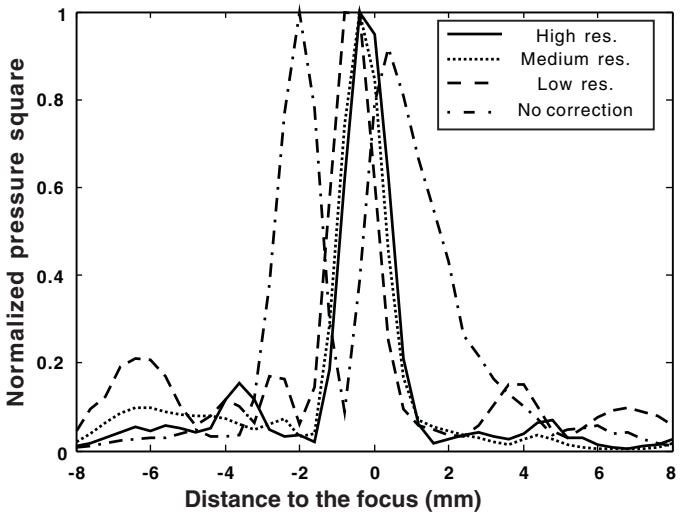

Figure 13. Pressure square distribution measurements along a line crossing the focal point for four different scenarios (high-resolution, medium-resolution, low-resolution k-space model and k-space propagation without the skull).

in therapeutic applications such as ablation of brain tumors. For comparison, a focused beam is created and back propagated in water; these signals are used to measure the ideal focus that can be obtained using the described technique and hardware. This ideal focus has a FWHM of 1.65 mm and side-lobe level at −12 dB. Even though results slightly vary, focusing signals computed with all three levels of resolution provide optimal focusing in the skull. Finally, the medium resolution is observed to have lower side lobes than the high-resolution case. This may possibly result from the registration between the array and the skull. The registration was done manually, therefore inevitably introducing errors. If these errors canceled out errors manifested from using the medium spatial resolution, this might make the medium-resolution case appear more accurate.

5. Conclusion

This paper investigated the feasibility of using a k-space method for transcranial beam focusing. Density data from CT images were used as the input to the numerical algorithm to simulate the wave propagation from a point source at the focal point. The received signal outside the skull was time reversed and sent back to the brain and created a sharp focus. Compared with the conventional FDTD method, which utilizes the finite difference to calculate the spatial derivative, the k-space method used the Fourier transform which resulted in a significantly reduced dispersion error even for a coarse spatial resolution.

A convergence study was first carried out for a quasi-plane wave propagation through the skull. Both the k-space method and FDTD method were tested. It was found that for very fine spatial resolution (more than ten grid points per wavelength), these two methods match very well. However, at a low spatial resolution, the k-space method was observed to produce considerably less numerical error. For this reason, we conclude that the k-space method is a rapid and accurate alternative to the FDTD method for transcranial focusing. This numerical and experimental study found that the k-space method implemented with a relatively low spatial resolution can still facilitate precise focusing inside the brain, without a significant loss of accuracy. This is advantageous, as a low spatial resolution indicates a short computation time. Indeed, the computation time at a fine spatial resolution (7.68 grid points per wavelength) can be reduced by a factor of around 80 if implemented at the lowest spatial resolution tested (2.56 grid points per wavelength).

In all current ongoing clinical trials, the phase aberration correction is performed while the patient is inside the MRI, just prior to treatment (McDannold *et al* 2010). In this case the MRI, CT and ultrasound reference frames are all co-registered. The significant time saved due to faster modeling could be highly beneficial from the standpoint of reduced patient stress as well as the time (and therefore cost) of an MR-guided procedure.

Acknowledgments

This work was supported by NIH grant R01 EB0003268.

References

Aubry J F, Tanter M, Pernot M, Thomas J L and Fink M 2003 Experimental demonstration of non-invasive trans-skull adaptative focusing based on prior computed tomography scans *J. Acoust. Soc. Am.* **113** 84–93

Behrens S, Spengos K, Daffertshofer M, Schroeck H, Dempfle C E and Hennerici M 2001 Transcranial-ultrasound-improved thrombolysis: diagnostic vs therapeutic ultrasound *Ultrasound Med. Biol.* **27** 1683–9

Clement G T and Hynynen K 2002a Correlation of ultrasound phase with physical skull properties *Ultrasound Med. Biol.* **28** 617–24

Clement G T and Hynynen K 2002b A non-invasive method for focusing ultrasound through the human skull *Phys. Med. Biol.* **47** 1219–36

Clement G T, White P J and Hynynen K 2004 Enhanced ultrasound transmission through the human skull using shear mode conversion *J. Acoust. Soc. Am.* **115** 1356–64

Cohen Z R, Zaubermann J, Harnof S, Mardor Y, Nass D, Zadicario E, Hananel A, Castel D, Faibel M and Ram Z 2007 Magnetic resonance imaging-guided focused ultrasound for thermal ablation in the brain: a feasibility study in a swine model *Neurosurgery* **60** 593–600

Colen R R and Jolesz F A 2010 Future potential of MRI-guided focused ultrasound brain surgery *Neuroimag. Clin. North Am.* **20** 355–66

Cox B, Arridge S R and Beard P C 2007 k-space propagation models for acoustically heterogeneous media: application to biomedical photoacoustics *J. Acoust. Soc. Am.* **121** 3453–64

Damianou C, Ioannides K, Hadjisavvas V, Mylonas N, Couppis A and Iosif D 2009 *In vitro* and *in vivo* brain ablation created by high-intensity focused ultrasound and monitored by MRI *IEEE Trans. Ultrason. Ferroelectr. Freq. Control* **56** 1189–98

Fink M and Prada C 2001 Acoustic time-reversal mirrors *Inverse Problems* **17** R1–38

Fry F J 1977 Transkull transmission of an intense focused ultrasonic beam *Ultrasound Med. Biol.* **3** 179–84

Gateau J, Marsac L, Pernot M, Aubry J F, Tanter M and Fink M 2010 Transcranial ultrasonic therapy based on time reversal of acoustically induced cavitation bubble signature *IEEE Trans. Biomed. Eng.* **57** 134–44

Hamilton M F and Blackstock D T 1998 *Nonlinear Acoustics* (San Diego, CA: Academic)

Haworth K J, Fowlkes J B, Carson P L and Kripfgans O D 2008 Towards aberration correction of transcranial ultrasound using acoustic droplet vaporization *Ultrasound Med. Biol.* **34** 435–45

Hynynen K, McDannold N, Vykhodtseva N, Raymond S, Weissleder R, Jolesz F A and Sheikov N 2006 Focal disruption of the blood–brain barrier by 260 kHz ultrasound bursts—a method for molecular imaging and targeted drug delivery *J. Neurosurg.* **105** 445–54

Jolesz F A 2009 MRI-guided focused ultrasound surgery *Annu. Rev. Med.* **60** 417–30

Jolesz F A, Hynynen K, McDannold N and Tempany C 2005 MR imaging-controlled focused ultrasound ablation: a noninvasive image-guided surgery *Magn. Reson. Imag. Clin. North Am.* **13** 545–60

Kinoshita M, McDannold N, Jolesz F and Hynynen K 2006 Noninvasive localized delivery of herceptin to the mouse brain by MRI-guided focused ultrasound-induced blood–brain barrier disruption *Proc. Natl Acad. Sci.* **103** 11719–23

Kosloff R and Kosloff D 1986 Absorbing boundaries for wave propagation problems *J. Comput. Phys.* **63** 363–76

Liu Q H 1998 The pseudospectral time-domain (PSTD) algorithm for acoustic waves in absorptive media *IEEE Trans. Ultrason. Ferroelectr. Freq. Control* **45** 1044–55

Marquet F, Pernot M, Aubry J F, Montaldo G, Marsac L, Tanter M and Fink M 2009 Non-invasive transcranial ultrasound therapy based on a 3D CT scan: protocol validation and *in vitro* results *Phys. Med. Biol.* **54** 2597–613

Martin E, Jeanmonod D, Morel A, Zadicario E and Werner B 2009 High-intensity focused ultrasound for noninvasive functional neurosurgery *Ann. Neurol.* **66** 858–61

Mast T D 2002 Two- and three-dimensional simulations of ultrasonic propagation through human breast tissue *Acoust. Res. Lett. Online* **3** 53–8

Mast T, Souriau L, Liu D, Tabei M, Nachman A and Waag R C 2001 A k-space method for large-scale models of wave propagation in tissue *IEEE Trans. Ultrason. Ferroelectr. Freq. Control* **48** 341–54

McDannold N, Clement G T, Black P M, Jolesz F A and Hynynen K 2010 Transcranial MRI-guided focused ultrasound surgery of brain tumors: initial findings in three patients *Neurosurgery* **66** 323–32

Meral F C and Clement G T 2010 128 element ultrasound array for transcranial imaging *IEEE Symp. on Ultrasonics* pp 1984–7

Pernot M, Aubry J F, Tanter M, Boch A L, Marquet F, Kujas M, Seilhean D and Fink M 2007 *In vivo* transcranial brain surgery with an ultrasonic time reversal mirror *J. Neurosurg.* **106** 1061–6

Pichardo S, Sin V W and Hynynen K 2011 Multi-frequency characterization of the speed of sound and attenuation coefficient for longitudinal transmission of freshly excised human skulls *Phys. Med. Biol.* **56** 219–50

Tabei M, Mast T D and Waag R C 2002 A k-space method for coupled first-order acoustic propagation equations *J. Acoust. Soc. Am.* **111** 53–63

Thomas J L and Fink M 1996 Ultrasonic beam focusing through tissue inhomogeneities with a time reversal mirror: application to trans-skull therapy *IEEE Trans. Ultrason. Ferroelectr. Freq. Control* **43** 1122–9

Tillet J C, Daoud M I, Lacefield J C and Waag R C 2009 A k-space method for acoustic propagation using coupled first-order equations in three dimensions *J. Acoust. Soc. Am.* **126** 1231–44

Treeby B E and Cox B T 2010 Modeling power law absorption and dispersion for acoustic propagation using the fractional Laplacian *J. Acoust. Soc. Am.* **127** 2741–8